Investigation of Influence of Medium pH and Sulfate Ion Concentrations on Corrosion Behavior of Magnesium Alloy ZE41

D. Nandini and A. Nityananda Shetty

Department of Chemistry, National Institute of Technology Karnataka, Surathkal, Srinivasnagar, Mangalore-575025, Karnataka, India, e-mail: nityashreya@gmail.com

Magnesium alloys have emerged as potential structural materials with all capabilities to even replace close contenders; aluminium alloys in weight-critical applications. High susceptibility to corrosion being the only limitation, corrosion of magnesium alloys continues to gather much attention among the material scientists worldwide. ZE41 is one such alloy of magnesium which is increasingly gaining importance as automobile and aerospace material. In the present study the influence of the medium pH and sulfate ion concentrations on the corrosion behavior of magnesium alloy ZE41 has been investigated using electrochemical techniques like the Tafel extrapolation and electrochemical impedance spectroscopy (EIS). The tests have been carried out in a range of conditions, with gradually varying pH and sulfate ion concentration. The morphology and composition of the corroded alloy surface have been determined by the scanning electron microscopy (SEM) and energy dispersion X-ray (EDX) analysis, respectively. The recorded results reflect a trend of a higher corrosion rate associated with a higher sulfate concentration at each pH and with a lower pH at each sulfate concentration.

Keywords: magnesium alloy ZE41, EIS, SEM, EDX.

УДК 620.197

INTRODUCTION

In recent times magnesium alloys have indeed received much attention as eco-friendly structural materials for automobiles and aircrafts, owing to their enviable physical properties combined with excellent recyclability. Apart from these well known applications, a class of magnesium alloys have also been pursued as electronic and bio-implant materials [1–3]. The advancement in technology has ensured development of newer magnesium alloys for tailor-made applications, however their high susceptibility to corrosion remains unabated and a limiting factor in their complete utility [4]. ZE41 is a magnesium alloy containing zinc, zirconium and rare earths (Mg-Zn-Zr-RE);it finds applications in various fields of modern engineering. Alloying Mg with Zn is known to improve the mechanical strength of both cast and wrought alloys. Zirconium is added to refine the grain size and addition of rare earth elements has been reported to improve the elevated temperature properties like creep performance [5]. In day-to-day outdoor applications the majority of ZE41 alloy parts get exposed to open atmosphere and often come under aqueous salt environments (acid rain and road splash for automobile parts) which are potential corrosives, setting severe corrosion of the alloy.

A detailed review of literature reveals studies carried out on several classes of magnesium alloys under varying conditions of medium pH. Song et al. [6] have investigated electrochemical corrosion of pure magnesium in 1N NaCl at different pH values. Tian et al. [7] have studied the corrosion behavior of magnesium alloy AZ91D in sodium sulfate solution with varying medium pH. Alteration of medium pH has also been employed to investigate the influence of microstructure [8–10] and different alloying elements [11] on the corrosion behavior of Mg alloys. The influence of pH and chloride ion concentration on corrosion of ZE41 alloy has been studied by Zhao et al. [12]. However the electrochemical corrosion behavior of ZE41 in varying pH and sulfate concentrations has not been documented. With that prospect present work is aimed at understanding the influence of the medium pH and sulfate ion concentration on corrosion of ZE41 magnesium alloy using electrochemical corrosion monitoring techniques.

EXPERIMENTAL

Material

The specimen investigated was magnesium alloy ZE41. The percentage composition of the alloy sample is displayed in Table 1. The cylindrical test coupon was prepared from as received rod shaped alloy by embedding in epoxy resin, such that a constant open surface area of 0.732 cm^2 is exposed to the corrosion medium during the experiment. This coupon was polished as per standard metallographic practice, belt grinding followed by polishing on emery papers of grades 600, 800, 1000, 1200, 1500, 2000, finally on polishing wheel using legated alumina abrasive to obtain mirror finish. The polished specimen was washed with double distilled water, degreased with acetone and dried before immersing in the sodium sulfate medium.

© D. Nandini and A. Nityananda Shetty, Электронная обработка материалов, 2014, **50**(2), 49–56.

Table 1. Composition of specimen (% by weight)

Element	% Composition	Element	% Composition
Zn	4.59	Sn	< 0.002
Ce	1.05	Pb	<0.002
Zr	0.7	Cu	< 0.002
La	0.48	Be	< 0.001
Pr	0.12	Ni	< 0.001
Mn	0.02	Cr	< 0.001
Nd	< 0.01	Sr	< 0.001
Fe	0.006	Mg	Balance
Al	0.004		

Medium

The electrolyte media of concentrations 0.2M, 0.6M and 1M were prepared using analytical grade sodium sulfate salt and double distilled water. The pH of the solution was adjusted to the desired value (pH = 2, 5, 7, 9, 12 for each sulfate concentration) with H_2SO_4 and NaOH, using a calibrated pH meter.

Electrochemical measurements

Electrochemical measurements were carried out using electrochemical work station, Gill AC having ACM instrument Version 5 software. A conventional three-electrode compartment Pyrex glass cell was used with a platinum counter electrode and a saturated calomel electrode (SCE) as reference. All the values of potential reported are referred to the SCE. The working electrode was made of ZE41 alloy specimen coupon. The polarization studies were done immediately after the electrochemical impedance spectroscopy (EIS) studies on the same exposed electrode surface without any additional surface treatment.

Potentiodynamic polarization studies

Well polished ZE41 alloy specimen coupon was exposed to the corrosion media, with varying pH and sulfate concentrations and allowed to establish a steady-state open circuit potential (OCP). The Tafel plots were recorded by polarizing the specimen to –250 mV cathodically and +250 mV anodically relative to the OCP at a scan rate of 1 mV s^{-1}.

Electrochemical impedance spectroscopy (EIS) studies

Impedance measurements were performed at the open circuit potential (OCP) by the application of a periodic small amplitude (10 mV) ac voltage signal with a wide spectrum of frequency ranging from 100 kHz to 0.01 Hz. The impedance data were analyzed using Nyquist plots. The double layer capacitance (C_{dl}) and charge transfer resistance (R_{ct}) were deduced from the analysis of Nyquist plots. In all of the above measurements, at least, three similar results were considered and their average values were reported.

Scanning Electron Microscopy (SEM) analysis

The surface morphology of the freshly polished ZE41 specimen, along with the corroded specimen exposed to acidic, neutral and alkaline Na_2SO_4 were obtained by recording SEM images of the corresponding samples using JEOL JSM-6380LA analytical scanning electron microscope.

RESULTS AND DISCUSSION

Potentiodynamic polarization measurements

The polarization studies of ZE41 alloy specimen were carried out in a range of conditions, with gradually varying pH and sulfate ion concentration, using the Tafel polarization method. The results confirm the influential role of the medium pH and sulfate ion concentrations in ZE41 alloy corrosion. Figure 1 represents the potentiodynamic polarization curves for the corrosion of ZE41 alloy in 0.2M Na_2SO_4 solutions with gradually varying pH. The potentiodynamic polarization curves for ZE41 alloy corrosion in neutral Na_2SO_4 solutions with varying sulfate concentrations are represented in Fig. 2. As seen from Fig. 1 and Fig. 2, polarization curves shift to the higher current density region, implying an increased corrosion rate as the medium pH decreases from highly alkaline (pH = 12) to highly acidic (pH = 2) conditions and as sulfate ion concentration increases from 0.2M to 1.0M, respectively. A similar trend of a higher corrosion rate associated with a lower medium pH was observed at other sulfate concentrations (0.6M and 1.0M), and the corrosion rate increased with the increased sulfate concentration at all measured pH, except pH 2. The linear Tafel behavior appeared only at cathodic branches of polarization curves, which are thought to represent cathodic hydrogen evolution through reduction of water. The anodic polarization curves did not exhibit the Tafel behavior, and are assumed to represent anodic oxidation of magnesium. However the cathodic branch of polarization curves showed linear Tafel behavior and is thought to represent the catho-

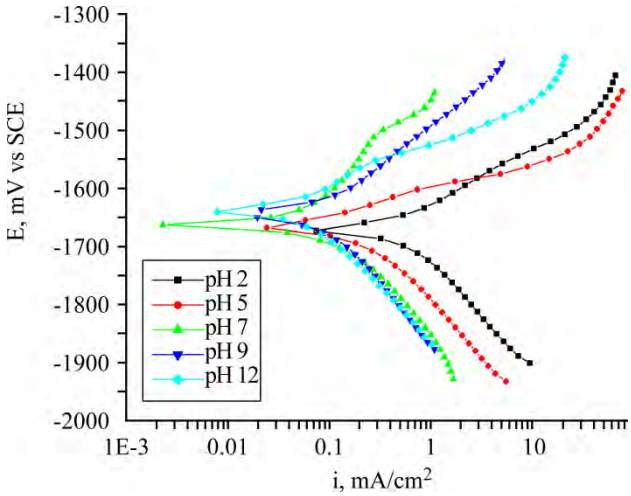

Fig. 1. Potentiodynamic polarization curves for corrosion of ZE41 alloy in 0.2M Na_2SO_4 solutions with varying pH.

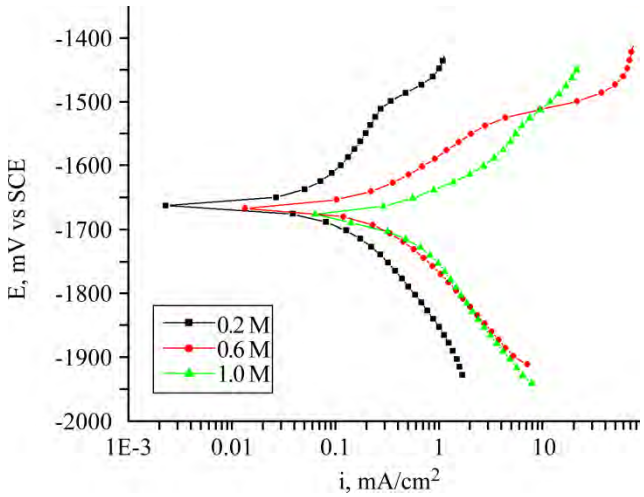

Fig. 2. Potentiodynamic polarization curves for corrosion of ZE41 alloy in neutral Na_2SO_4 solutions with varying sulfate concentrations.

Table 2. Electrochemical polarization parameters for corrosion of ZE41 alloy in Na_2SO_4 solutions with gradually varying pH and sulfate ion concentration

Na_2SO_4 concentration [M]	pH	E_{corr} [mV]	i_{corr} [μA/cm^2]	$-b_c$ [mV/dec]	υ_{corr} [mm/year]
	2	-1670	534	209	12.0
	5	-1664	242	205	5.4
0.2	7	-1662	124	207	2.8
	9	-1643	89	204	2.0
	12	-1638	59	180	1.3
	2	-1673	658	208	15.0
	5	-1675	419	197	9.3
0.6	7	-1663	276	182	6.2
	9	-1655	212	182	4.7
	12	-1651	176	179	3.9
	2	-1689	903	216	20.1
	5	-1681	637	209	14.2
1	7	-1681	499	237	11.1
	9	-1668	364	200	8.1
	12	-1665	317	198	7.1

dic hydrogen evolution through reduction of water.

The potentiodynamic polarization curves obtained were further analyzed by the Tafel extrapolation of the cathodic braches of the Tafel plot to the OCP to obtain the corrosion current density (i_{corr}). The potentiodynamic polarization parameters like corrosion potential (E_{corr}), corrosion current density (i_{corr}), cathodic slope (b_c) were calculated from the Tafel plots. The corrosion rate (υ_{corr}) was calculated using the following equation:

$$\upsilon_{corr}\left(\text{mmy}^{-1}\right)=\left(3270\cdot \text{M}\cdot i_{corr}\right)/\left(\rho\cdot Z\right) \qquad (1)$$

where, 3270 is a constant that defines the unit of the corrosion rate (mmy^{-1}), i_{corr} is the corrosion current density in A·cm^{-2}, ρ is the density of the corroding material, in this case density of ZE41 alloy 1840 kg·m^{-3}, M is the atomic mass of the metal, and Z is the number of electrons transferred per metal atom [13]. The deduced potentiodynamic polarization parameters like E_{corr}, i_{corr}, b_c and the calculated υ_{corr} are presented in Table 2.

The Pourbaix diagram for pure magnesium as shown in Fig. 3 [14], best explains the corrosion behavior of magnesium and its alloys in a wide range of pH. This potential-pH plot represents of the stability of metallic magnesium and its corrosion product magnesium hydroxide ($Mg(OH)_2$) as a function of the potential and pH (acidity or alkalinity) of aqueous solutions. The corrosion mechanism of magnesium can be summarized in following corrosion reactions[15]:

$$\text{Mg}\rightarrow \text{Mg}^{2+}+2e^{-}, \qquad (2)$$

$$2\text{H}_2\text{O}+2e^{-}\rightarrow \text{H}_2+2\left(\text{OH}\right)^{-}, \qquad (3)$$

$$\text{Mg}^{2+}+2\text{OH}^{-}\rightarrow \text{Mg}\left(\text{OH}\right)_2. \qquad (4)$$

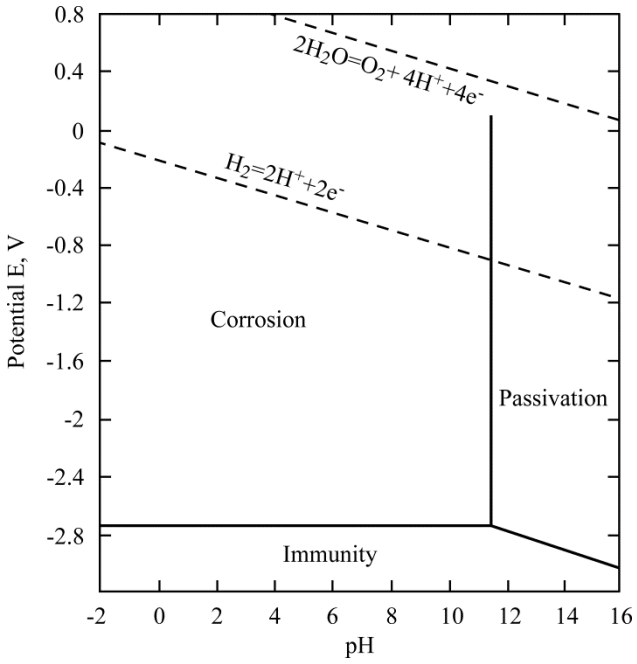

Fig. 3. Potential-pH (Pourbaix) diagram for the system of magnesium and water at 25ºC, showing theoretical domains of corrosion, immunity, and passivation. Source: Ref 14.

The anodic reaction involves dissolution of magnesium, the cathodic reaction is hydrogen evolution by reduction of water, that owing to the low solubility of Mg^{2+}, $Mg(OH)_2$ precipitates creating a surface layer on the corroding metal. The Pourbaix diagram supposes the corrosion product $Mg(OH)_2$ to be stable only in alkaline conditions, with pH above 10.5, but even though $Mg(OH)_2$ is thermodynamically unstable at pH below 10.5, metallic magnesium can readily develop $Mg(OH)_2$ surface film even at acidic pH values, if the dissolution rate of $Mg(OH)_2$ is lower than the rate of its formation. Moreover as a result of the cathodic reaction of hydroxyl ion generation, an alkaline pH zone develops at the electrode interface, which facilitates $Mg(OH)_2$ precipitation and film formation, even when the bulk pH is acidic [12].

With the understanding of the mechanism, it is safe to justify the observed trend of the increased corrosion rate of ZE41 alloy with the decrease of pH at every sulfate concentration tested. At alkaline conditions the $Mg(OH)_2$ surface film is highly stable and protective, resulting in a reduced corrosive attack. Lowering medium pH increases the solubility of the surface film, which accounts for high corrosion rates in acidic media. However, the corrosion rate observed in alkaline media is significant, though small; this is because the $Mg(OH)_2$ surface film is thin with a Pilling-Bedworth ratio ~ 0.81 [16] and the film is partially protective, hence incapable of imparting complete passivity to the underlying metal, so corrosion reactions take place predominantly at the breaks and imperfections of the film [17–19].

As shown in Table 2, that corrosion rate of ZE41 alloy increases with the increase of sulfate concentration at each pH, which is in agreement with the commonly observed trend, that reflects the influence of the corrosive strength on the corrosion rate of the alloy. Sulfate and several other anions like chloride and bromides increase the fraction of the film-free surface and produce breaks and imperfections in the surface film, which accounts for their strong corrosive nature towards magnesium alloys [20]. Several studies [21–23] have established sulfate as an appreciably strong corrosive for magnesium alloys and the results of the authors of the given article are in agreement with that finding. Also both E_{corr} and b_c gradually change with varying pH and sulfate concentration, which shows that both factors do influence on the kinetics of cathodic hydrogen evolution and anodic metal dissolution reactions.

Electrochemical impedance spectroscopy

The impedance results are helpful in understanding electrochemical interfaces. The impedance measurements of the ZE41 alloy specimen were carried out under similar conditions as stated in the previous section. Figure 4 presents Nyquist plots for the corrosion of ZE41 alloy in 1.0M Na_2SO_4 solutions, with gradually varying pH. Figure 5 shows Nyquist plots for the corrosion of ZE41 alloy in acidic Na_2SO_4 solutions with pH 2 and varying sulfate concentrations. Those Nyquist plots are comprised of two capacitive loops at higher and medium frequencies, followed by the beginning of an inductive loop at a lower frequency region. A higher frequency (HF) semicircle has been attributed to the charge transfer of the corrosion process and oxide film effects; a medium frequency (MF) semicircle – to mass transport (diffusion of magnesium ions) in the solid phase through the corrosion product layer; and a lower frequency (LF) inductive loop – to relaxation of surface adsorbed species like $Mg(OH)^+$ and $Mg(OH)_2$. This pattern of Nyquist plots appears characteristic of magnesium alloys [21, 24]. The charge transfer resistance (R_{ct}) and the double layer capacitance (C_{dl}) are deduced from the analysis of a higher frequency capacitive loop [25–26].

The corrosion current density is calculated using the Stern Geary equation below.

$$i_{corr} = b_a b_c / 2.3\left(b_a + b_c\right) R_{ct}. \qquad (5)$$

It is evident from the representative plots shown in Fig. 4 and Fig. 5 that the diameter of the HF semicircle decreases with the increase in the strength of Na_2SO_4 and with decrease in pH implying an increase in the rate of corrosion. Similar plots have been obtained under all other tested conditions. The results of EIS measurements; R_{ct}, C_{dl} and υ_{corr} are summarized in Table 3.

The impedance results are analyzed using equivalent circuit models. The circuit fitment was done by

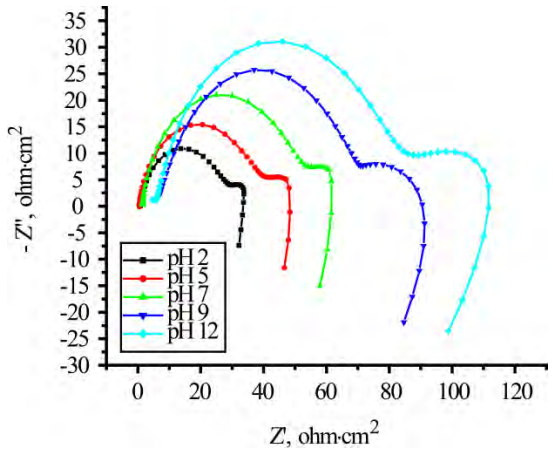

Fig. 4. Nyquist plots for corrosion of ZE41 alloy in 1.0M Na_2SO_4 solutions with varying pH.

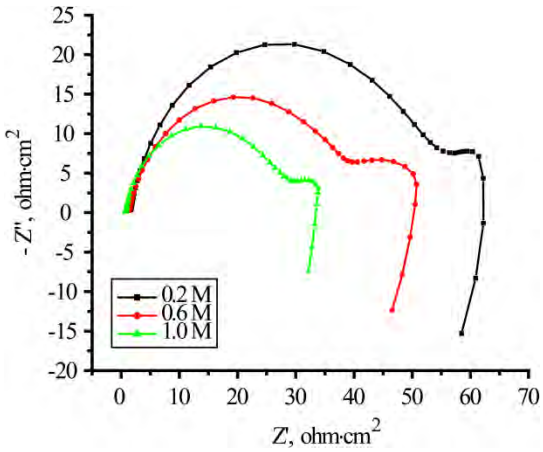

Fig. 5. Nyquist plots for ZE41 alloy corrosion in acidic Na_2SO_4 solutions with pH 2 and varying sulfate concentrations.

Table 3. Impedance parameters for corrosion of ZE41 alloy in Na_2SO_4 solutions with gradually varying pH and sulfate ion concentration

Na_2SO_4 concentration [M]	pH	R_{ct} [Ω cm^2]	C_{dl} [μF/cm^2]	υ_{corr} [mm/year]
	2	53.7	22.4	10.8
	5	120.6	22.1	4.8
0.2	7	213.9	21.4	2.7
	9	306.9	18.5	1.9
	12	377.5	17.2	1.5
	2	39.5	23.3	14.7
	5	58.3	21.2	10.0
0.6	7	93.3	21.4	6.2
	9	122.0	20.1	4.8
	12	188.6	18.8	3.1
	2	27.8	25.0	20.9
	5	38.9	24.5	14.9
1	7	51.6	19.6	11.3
	9	65.0	19.1	8.9
	12	78.5	18.7	7.4

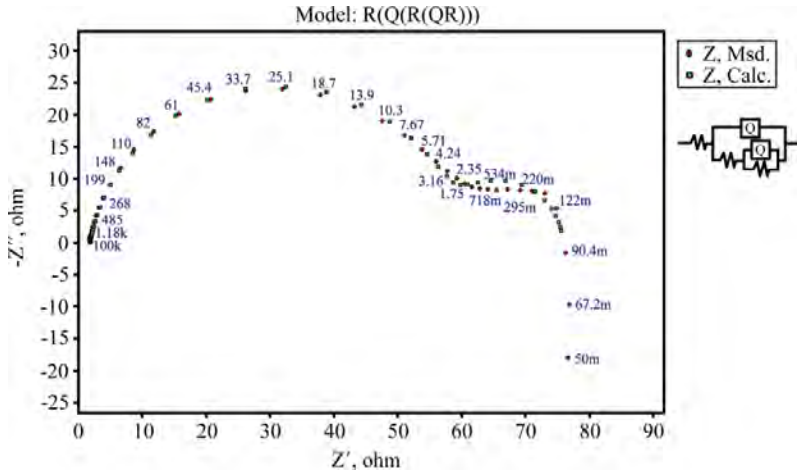

Fig. 6. Simulation of experimental impedance data points with theoretical model for corrosion of ZE41 alloy specimen in 0.6M Na_2SO_4 solution with pH 5.

the ZSimpWin software of version 3.21. Figure 6 shows the simulation of the impedance data points. The equivalent circuit modeling the electrochemical behavior of the interface as shown at the right hand corner of Fig. 6 comprises five circuit elements, R_s represents the solution resistance, R_{ct} stands for the charge transfer resistance. The capacitive loops appear as depressed semicircles, as a result of frequency dispersion arising due to inhomogeneity of solid surfaces [27]. The constant phase element (Q_{dl}) is

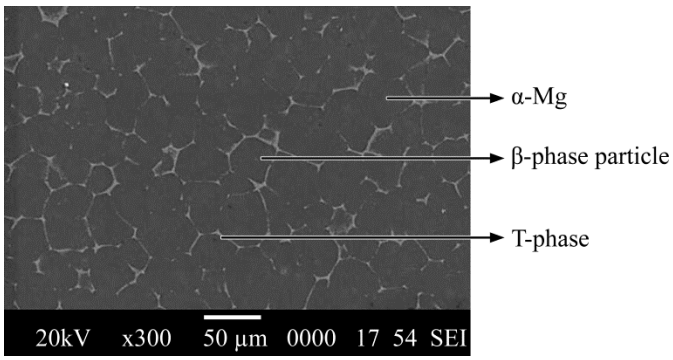

Fig. 7a. SEM image of freshly polished surface of ZE41 alloy specimen.

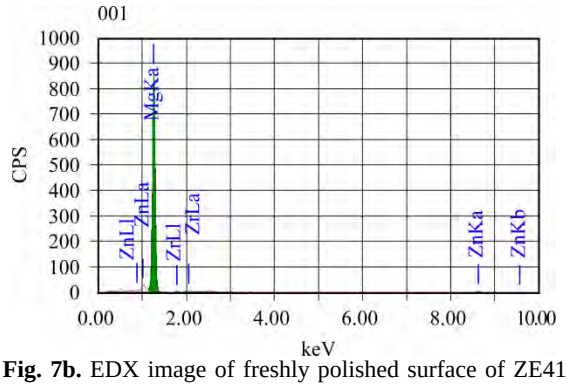

Fig. 7b. EDX image of freshly polished surface of ZE41 alloy specimen.

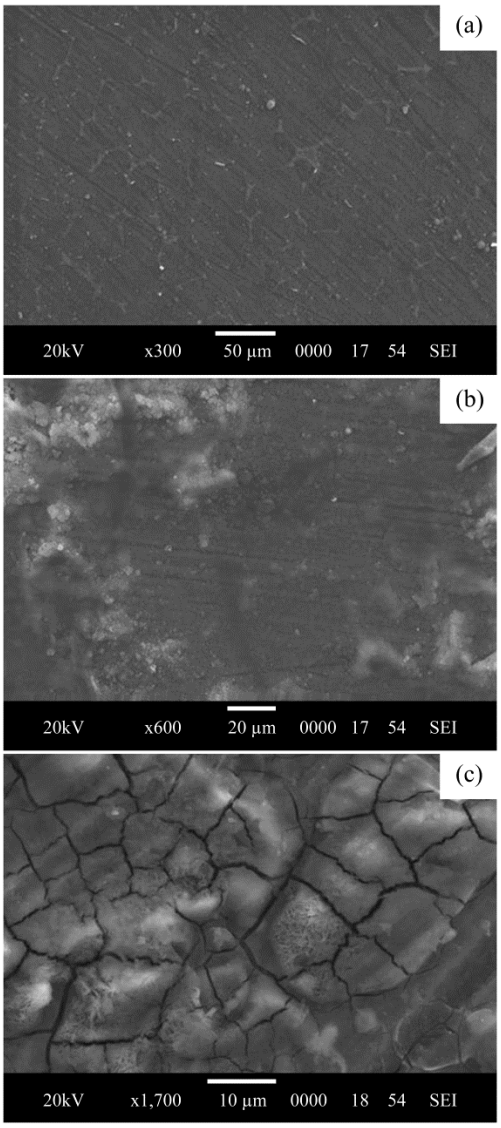

Fig. 8. SEM image of ZE41 specimen surface after 1 hour immersion in (a) acidic 1M Na_2SO_4 with pH 2; (b) neutral 1M Na_2SO_4 and (c) alkaline 1M Na_2SO_4 with pH 12.

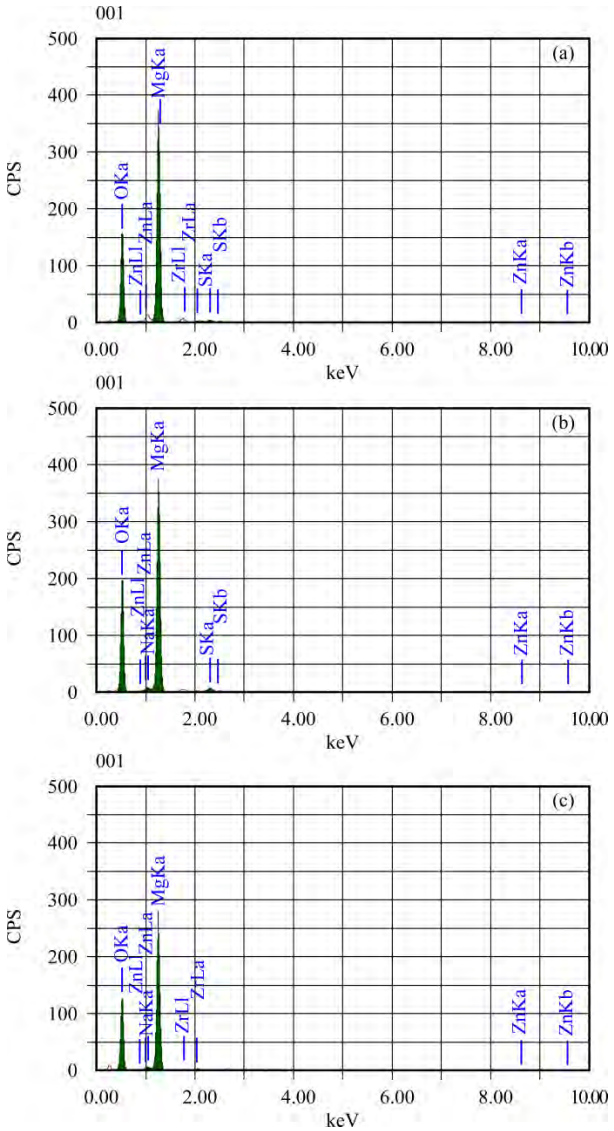

Fig. 9. EDX image of ZE41 specimen after 1 hour immersion in (a) acidic 1M Na_2SO_4 with pH 2; (b) neutral 1M Na_2SO_4 and (c) alkaline 1M Na_2SO_4 with pH 12.

substituted for the ideal capacitive element to account for this unevenness and porosity of the electrode surface. The impedance of the constant phase is described by the expression:

$$Z_Q = Y_0^{-1}(j\omega)^{-n} \qquad (9)$$

where Y_0 is the CPE constant, ω is the angular frequency (in rad s^{-1}), j^2 = -1, is the imaginary number and n is a CPE exponent that is a measure of the heterogeneity or roughness of the surface.

Scanning electron microscopy

The surface morphology of the alloy is often helpful in estimating the effect of a corrosive and pH on the alloy surface. The surface morphology was analyzed in the given study by the scanning electron

microscopy (SEM). The SEM image of a freshly polished surface of a ZE41 alloy is shown in Fig. 7a. The surface appears uniform and the microstructure of the alloy consisting of the α-Mg matrix along with randomly distributed second phase (β-phase) particles and the T-phase occurring along the grain boundaries [28] is evident. The energy dispersion X-ray (EDX) image of a freshly polished surface of a ZE41 alloy is shown in Fig. 7b.

Figures 8a,b and c are SEM images of the ZE41 specimen surface after 1 hour of immersion in an acidic medium 1M Na_2SO_4 with pH 2, in neutral 1M Na_2SO_4 and alkaline 1M Na_2SO_4media with pH 12, respectively. The surface appears corroded and the reduced visibility of the microstructure suggests the existence of a surface film. The sample immersed in an alkaline medium showed the thickest deposition, as presumed due to a reduced solubility of $Mg(OH)_2$. The surface layers of all samples are non-uniform. The EDX images of the corroded surface are shown in Figs. 9a,b and c for specimens immersed in an acidic, neutral and alkaline Na_2SO_4, respectively. A strong peak of oxygen in EDX patterns is exclusive to corroded specimens and knowing the corrosion mechanism, the film on the surface can be said to comprise deposits of the hydrated magnesium oxide ($MgO{\cdot}H_2O$) and magnesium hydroxide ($Mg(OH)_2$).

CONCLUSIONS

1. The corrosion behavior of a magnesium alloy ZE41 in Na_2SO_4 solutions is strongly influenced by both medium strength and its pH.

2. A higher corrosion rate is associated with a higher sulfate ion concentration at each pH and with a lower pH at each sulfate ion concentration.

3. The ZE41 alloy exhibited the highest rate of corrosion in 1M Na_2SO_4pH 2 medium and the lowest in 0.2M Na_2SO_4 pH 12 solution.

4. The results of the electrochemical investigation, SEM and EDX analyses collectively convey the presence of a partially protective $Mg(OH)_2$ surface film that single-handedly influences the corrosion behavior of a ZE41 alloy.

REFERENCES

1. Aghion E., Bronfin B., Von B.F., Schumann S., Friedrich H. Newly Developed Magnesium Alloys for Powertrain Applications. *JOM*. 2003, **55**(11), 30–33.
2. Agnew S.R. Wrought Magnesium: A 21st Century Outlook. *JOM*. 2004, **56**(5), 20–21.
3. Gupta M. and Sharon N.M.L. *Magnesium, Magnesium Alloys and Magnesium Composites*. New Jersy: John Wiley & Sons, 2011. 265 p.
4. Blawert C., Hort N. and Kainer K.U. Automotive Applications of Magnesium and its Alloys. *Trans Indian Inst Met*. 2004, **57**, 397–408.
5. Rzychoń T. And Kiełbus A. Effect of Rare Earth Elements on the Microstructure of Mg-Al Alloys. *JAMME*. 2006, **17**, 1–2.
6. Song G., Atrens A., Stjohn D., Nairn J. and Li Y. The Electrochemical Corrosion of Pure Magnesium in 1N NaCl. *Corros Sci*. 1997, **39**, 855–875.
7. Tian Y., Yang L., Li Y.F., Wei Y., Hou L., Li Y.G. and Murakami R. Corrosion Behavior of Die-cast AZ91D Magnesium Alloys in Sodium Sulphate Solutions with Different pH Values. *Trans Nonferrous Met Soc China*. 2011, **21**, 912–920.
8. Mathieu S., Rapin C., Steinmetz J. and Steinmetz P. A Corrosion Study of the Main Constituent Phases of AZ91 Magnesium Alloys. *Corros Sci*. 2003, **45**, 2741–2755.
9. Song G., Atrens A. and Dargusch M. Influence of Microstructure on the Corrosion of Diecast AZ91D. *Corros Sci*. 1999, **41**, 249–273.
10. Song G., Atrens A., Wu X. and Zhang B. Corrosion Behavior of AZ21, AZ501 and AZ91 in Sodium Chloride. *Corros Sci*. 1998, **40**, 1769–1791.
11. Lisitsyn V., Ben-Hamu G., Eliezer D. and Shin K.S. Some Particularities of the Corrosion Behavior of Mg-Zn-Mn-Si-Ca Alloys in Alkaline Chloride Solutions. *Corros Sci*. 2010, **52**, 2280–2290.
12. Zhao M.C., Liu M., Song G. and Atrens A. Influence of pH and Chloride Ion Concentration on the Corrosion of Mg Alloy ZE41.*Corros Sci*. 2008, **50**, 3168–3178.
13. Fontana M.G. *Corrosion Engineering*. Singapore: McGraw Hill, 1987. pp. 173.
14. Pourbaix M. *Atlas of Electrochemical Equilibria Aqueous Solutions*. Houston: NACE, 1974.pp. 139.
15. Baghni M., Wu Y., Li J. and Zhang W. Corrosion Behavior of Magnesium and Magnesium Alloys. *Trans Nonferrous Met Soc China*. 2004, **14**, 1–10.
16. Guo K.W. A Review of Magnesium/Magnesium Alloy Corrosion and its Protection. *Recent Patents on Corros Sci*. 2010, **2**, 13–21.
17. Song G. and Atrens A. Corrosion Mechanisms of Magnesium Alloys. *Adv Eng Mater*. 1999, **1**(1), 11–33.
18. Song G. and Atrens A. Understanding Magnesium Corrosion – A Framework for Improved Alloy Performance. *Adv Eng Mater*. 2003, **5**(12), 837–858.
19. Song G. and Atrens A. Recent Insights into the Mechanism of Magnesium Corrosion and Research Suggestions. *Adv Eng Mater*. 2007, **9**(3), 177–183.
20. Godard H.P., Jepson W.P., Bothwell M.R. and Kane R.L. *The Corrosion of Light Metals*. New Jersy: John Wiley & Sons, 1967. 372 p.
21. Baril G., Galicia G., Deslouis C., Pebere N., Tribollet B. and Vivier V. An Impedance Investigation of the Mechanism of Pure Magnesium Corrosion in Sodium Sulfate Solutions. *J Elecrochem Soc.* 2007, **154**(2), 108–113.

22. Song G., Atrens A., Stjohn D., Wu X. and Nairn J. The Anodic Dissolution of Magnesium in Chloride and Sulphate Solutions. *Corros Sci*. 1997, **39**, 10–11.

23. Wang L., Shinohara T. and Zhang B. Influence of Chloride, Sulfate and Bicarbonate Anions on the Corrosion Behavior of AZ31 Magnesium Alloy. *J Alloys Compds*. 2010,**496**, 500–507.

24. Baril G. and Pebere N. The Corrosion of Pure Magnesium in Aerated and Deaerated Sodium Sulphate Solutions. *Corros Sci*. 2001, **43**, 471–484.

25. Song G. and Stjohn D. Corrosion Behavior of Magnesium in Ethylene Glycol. *Corros Sci*. 2004, **46**, 1381–1399.

26. Ardelean H., Frateur I. and Marcus P. Corrosion Protection of Magnesium Alloys by Cerium, Zirconium and Niobium-based Conversion Coatings. *Corros Sci*. 2008, **50**, 1907–1918.

27. Jüttner K. Electrochemical Impedance Spectroscopy (EIS) of Corrosion Processes on Inhomogeneous Surfaces. *Electrochimica Acta*. 1990, **35**(10), 1501–1508.

28. Neil W.C., Forsyth M., Howlett P.C., Hutchinson C.R. and Hinton B.R.W. Corrosion of Magnesium Alloy ZE41 – The Role of Microstructural Features. *Corros Sci*. 2009, **51**, 387–394.

Received 24.12.12
Accepted 11.03.13

Реферат

Магниевые сплавы являются многообещающим конструкционным металлом и остаются главным конкурентом алюминиевых сплавов в областях, где важны весовые характеристики. Их основной недостаток – высокий уровень подверженности коррозии, поэтому борьба с коррозией магниевых сплавов находится в центре внимания исследователей в области материаловедения во всем мире. Сплав Mg-Zn-RE (ZE41) часто используется в автомобильной промышленности и авиастроении. Целью данной работы было изучение влияния водородного показателя (pH) среды и концентрации ионов сульфата аммония на устойчивость к коррозии сплава ZE41. Применялись такие известные в электрохимии методики, как импедансная электрохимическая спектроскопия и поляризационные измерения. Опыты проводились при постепенном изменении pH и концентрации ионов сульфата аммония. Структура и состав поверхности сплава, подвергшегося коррозии, анализировались с помощью сканирующего электронного микроскопа и рентгеноструктурного анализатора на основе метода энергетической дисперсии, соответственно. Полученные результаты отражают тенденцию к увеличению скорости коррозии при повышении концентрации ионов сульфата аммония и заданном pH, или при уменьшении pH и при заданной концентрации ионов сульфата аммония.

Ключевые слова: магниевый сплав ZE41, импедансная электрохимическая спектроскопия (EIS), сканирующая электронная микроскопия (SEM), рентгеноструктурный анализ на основе метода энергетической дисперсии (EDX).